Chapter 5

ELNES of graphite, diamond and binary boron, silicon and carbon nitrides

In this chapter the experimental K-shell near-edge structure (NES) and multiple-scattering (MS) calculated NES are compared for the diamond and graphite, and the binary nitrides of boron (c-BN and h-BN) and silicon (β-Si_3N_4) to validate the reliability of the MS approach. The MS approach reproduces the positions of major features to within 2eV. The MS calculated NES for hypothetical β-C_3N_4 is also presented, without direct experimental comparison. The MS spectra should serve as a fingerprint for identifying phases of carbon nitrides in the search for crystalline-C_3N_4.

5.1 Introduction

Many experimental methods have been developed to probe the physical and electronic structure of materials. These methods seek to understand the relationships between the measured structural information and the properties of the material. As discussed in Chapter 2, Electron Energy Loss Spectroscopy (EELS) is a useful technique because it

can probe local bonding effects of specific atomic species in a multi-component atomic system. One reason for the emphasis in this thesis on EELS is its excellence in identifying and quantifying chemical composition and structural detail for light elements such as carbon and nitrogen.

In Chapter 1 the difficulties in identifying crystalline C_3N_4 was discussed, particularly the lack of complete characterisation of carbon nitride materials in either diffraction and/or elemental composition to unambiguously identify it. Chronologically, the work in this chapter was performed soon after the deposition work of Chapter 3 as a possible aid to characterising crystalline carbon nitride materials. One motivation for this study was also to determine if present experimental EELS spectra was consistent with the proposed structures of β-C_3N_4.

Therefore in this chapter the work is presented as follows. Firstly the experimental C K-edge ELNES for diamond and graphite is compared to the MS calculated spectra. This is followed by a section on boron nitrides (BN) for several reasons; BN is one candidate for an ultra-hard material ; c-BN/h-BN are structurally analogous to diamond/graphite; This means BN is a good second system to compare MS calculations to experiment. The third section of this chapter covers the N K-edge for β-Si_3N_4, before finally comparing and discussing the ELNES of Carbon and Nitrogen in β-C_3N_4. To begin with the MS approach for calculation of ELNES is discussed in detail.

5.2 Background

In addition to providing elemental concentrations, the characteristic absorption edges in electron energy loss (EEL) spectroscopy contains fine structure which holds information on the local atomic environment of the absorbing atom [1].

5.2.1 ELNES

As shown in fig(5.1), the electron energy-loss spectrum can be divided into two regions; the energy-loss near-edge structure (ELNES) and the extended energy-loss fine structure (EXELFS). ELNES is the region within 30-40eV of the edge onset, and is

the modulation of the basic edge shape reflecting the local density of unoccupied states (LDOS). For example, in the figure(5.1), the strong pre-edge feature at 285eV corresponds to 1s-π^* transitions, and is associated with conduction π states around M and L points in the Brillouin Zone of graphite [2]. In this sample - glassy carbon - this feature indicates sp and sp^2 hybridisation of carbon. ELNES can also be used for coordination "fingerprinting", and can be used to identify phases in complex systems as shown by Brydson *et al.* [3, 4, 5] or phase changes over a nanometre scale as shown by Redlich *et al.* [6] who studied the effects of irradiation on carbon "onions" .

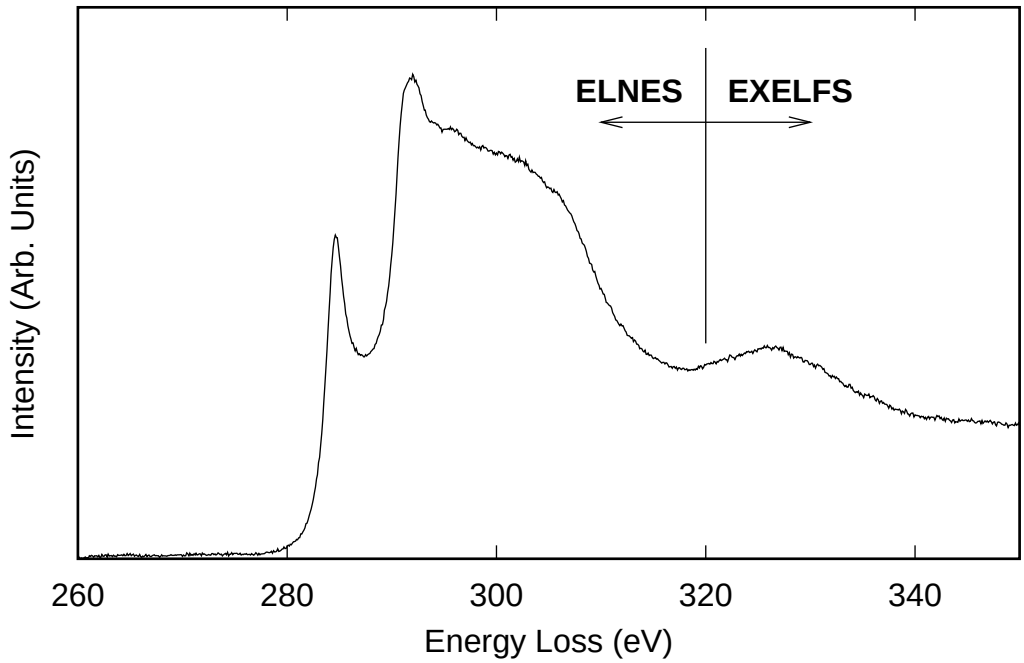

Figure 5.1: The experimental carbon K-edge ELNES from glassy carbon. The approximate regions of ELNES and EXELFS are marked on the diagram.

5.2.2 Difference between ELNES and EXELFS

Beyond ≈30–40eV of the absorption edge, the EXELFS region is produced by single elastic scattering of the ejected electron from neighbouring atoms. The principal reason for the distinction or difference between EXELFS and ELNES is in terms of scattering theory. In the near-edge region, the 1s electron ejected by an energy-loss event has low kinetic energy which allows sampling of a larger volume of material, and allows multiple elastic scattering from surrounding atoms [3]. EXELFS is produced by electrons with

higher kinetic energy, and single scattering from nearest-neighbours dominates. The modulations in the EXELFS region of a spectrum can extend for several hundreds of eV, and can be analysed to give a form of radial distribution function. The theory of EXELFS is well understood, although its experimental application is difficult due to problems including signal-to-noise and electron-probe stability over the long collection times necessary [1].

5.2.3 Calculation of ELNES

In an energy loss event, an electron scatters from a core electron (as described earlier in Section(2.4)) losing energy (ΔE). This energy ΔE is transferred to the ejected core electron, increasing its energy above the Fermi energy.

The outgoing spherical electron wavefunction can be treated in two ways as shown in fig (5.2)). One way is to treat the event as a time-dependant perturbation to the atom, modelling the transition from initial to final state wavefunction, essentially "sampling" the unoccupied density of states. In this way the basic edge shape is defined by atomic physics and is independent of the local environment of bonding of the atom, but modified by the local density of states.

A different way of approaching the problem is to consider the interference of the outgoing spherical wave as it is multiply scattered from surrounding atoms. This is the Multiple Scattering (MS) technique which is performed on a structure in real space which can be useful in disordered systems. MS has been shown to be equivalent to Korringa-Kohn-Rostocker (KKR) band theory [7] methods, which are performed in reciprocal space. The MS approach allows a shell-by-shell calculation which would not be possible in a reciprocal space calculation.

5.3 The MS Calculation

The MS approach was originally used for the calculation of X-ray absorption near-edge structure (XANES). The MS method can also be used for the calculation of ELNES because of the small collection angles with correspondingly small momentum transfer,

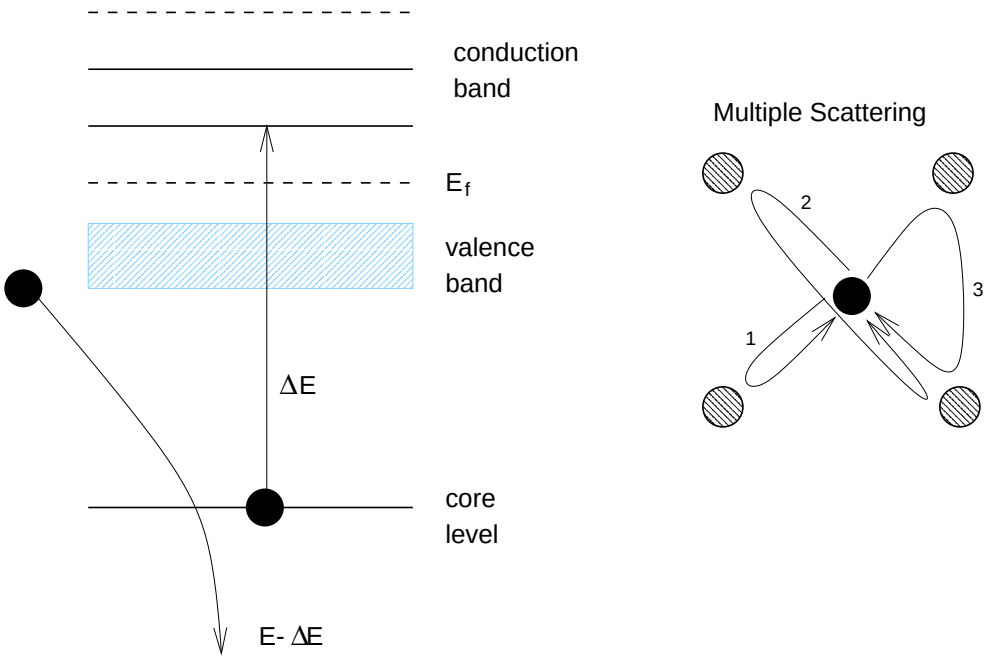

Figure 5.2: The two equivalent ways of treating ELNES are (i) the density of states and (ii) multiple-scattering in which outgoing spherical electron wave interferes with itself as it scattering from surrounding atomic potentials.

where dipole transitions dominate.

The MS technique was implemented in the IC-XANES program written by Durham-Pendry-Hodges [8] and Vvedensky, Saldin and Pendry [9]. The inputs to the program are shown diagrammatically by fig(5.3) which shows the different programs used, and indicates the flow of information between the different codes. The inputs can be divided into three sections. The first are the crystal coordinates and symmetry which form a cluster coordinates of atoms. This cluster is subdivided into concentric shells each containing atoms separated by no more than 1Å. The second input is the matrix elements for the electron transition from an atomic 1s state (in the case of a K edge calculation) to the conduction band state. The conduction band state is calculated by solving the one electron Schrödinger equation for an array of muffin-tins. The third major input is the phase shifts for incident spherical waves with angular momenta up to $l_{max} = 3$, describing the scattering properties of each atom.

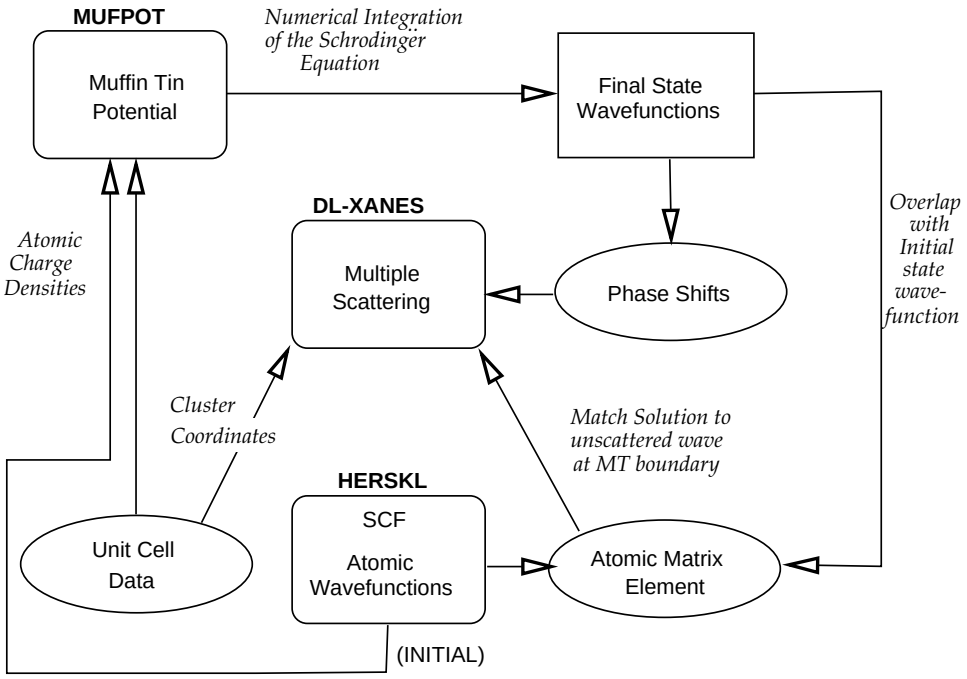

Figure 5.3: The ELNES calculation using MS involves the cooperation between three different programs: HERSKL, MUFPOT and IC-XANES. This diagram shows the flow of information between the three programs to produce the final calculation. Reproduced from Brydson [10].

5.3.1 Dipole Selection Rules

The differential scattering cross-section with a momentum transfer of $\mathbf{q}$, as described by Fermi's Golden Rule [1] is:

$$\frac{d^2I}{d\Omega dE} = \frac{4\gamma^2}{a_o^2 q^4} | < f \, | exp(i\mathbf{q}\cdot\mathbf{r}) | i > |^2 \, \rho(E) \tag{5.1}$$

in which γ is the relativistic correction, a_o the Bohr radius, q is the momentum transfer, $\rho(E)$ the density of final states, and $< i|$ and $|f >$ represent the initial and final wavefunctions respectively. This cross-section assumes that fast electron states can be expressed as plane waves [1].

For ELNES, the product $\mathbf{q} \cdot r \ll 1$, the exponential is expanded to first order. This is because $\mathbf{r}$ s given by the spread of the initial wavefunction (for K-shell this is a 1s, L-shell a 2p). As the initial and final wavefunctions can be written as products of radial wavefunctions and spherical harmonics, the angular integration produces what

are known as the dipole selection rules:

$$l' = l \pm 1 \qquad \text{and} \qquad \Delta j = 0, \pm 1 \qquad \text{(j=l+s)} \tag{5.2}$$

in which l and l' are the initial and final wavefunction angular momentum. For small momentum transfer ($q \to 0$) transitions follow these dipole selection rules.

The initial wavefunction is a localised core level corresponding to the absorption edge (K, L, M etc). The final state is a spherical wavefunction originating on the absorbing atom. As this spherical wavefunction propagates, it is reflected from surrounding atomic potentials and returns to interferes with the outgoing wavefunction. The interference between these waves gives rise to the variation in near-edge structure.

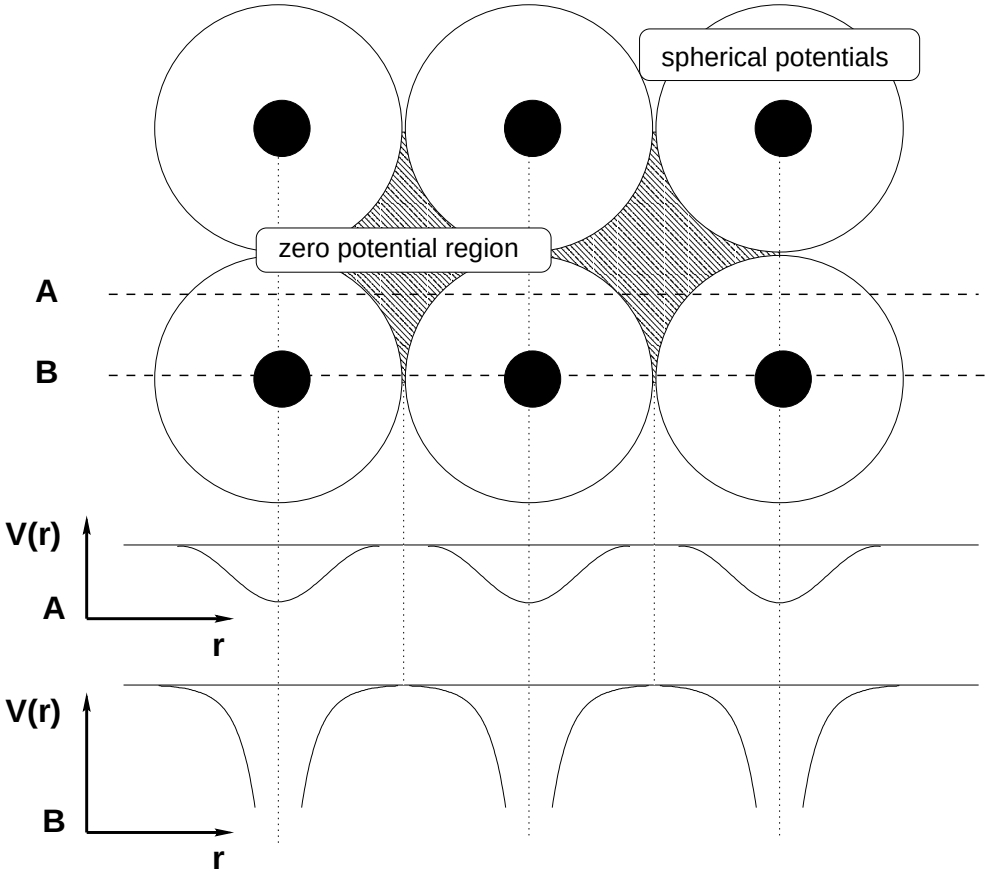

Figure 5.4: Schematic representation of the "muffin tin" crystalline potential, inside the muffin-tins the atomic potential is spherically averaged, while outside the potential is volume averaged. Reproduced from Brydson [10].

5.3.2 Atomic Wavefunction Calculations

The initial atomic wavefunctions are determined using self-consistent Hartree-Slater (H-S) wavefunctions for isolated atoms. The method of Herman and Skillman was implemented for this step [11].

These H-S wavefunctions are then used together with the atomic coordinates to form the coulombic potential of the atomic array. These atomic potentials are spherically averaged, and their extent confined to muffin-tins around each atomic centre. The radius of the muffin tin is chosen to ensure there is no overlap between adjacent muffin-tins, and that the potential inside the muffin tin matches smoothly with the average potential without, as shown in fig(5.4) according to the Mattheiss Prescription.

The Mattheis Prescription [12] is that spherically symmetric contributions from the atomic potentials of all neighbouring atoms are superposed on the atomic potential of the central atom to yield its muffin-tin potential.

The one electron Schrödinger equation is then solved numerically for the array of muffin-tins. The exchange-correlation is accounted for using the local-density approximation with the local exchange parameter α=0.8 [13]. Then, together with the initial core H-S wavefunctions and the final state wavefunctions, the transition matrix $M(E)$ is evaluated.

A dipole matrix element $M_{c,L}(E)$ is defined by:

$$M_{c,L}(E) = \int dr R_l(r,E) Y_L(\hat{r}) \Delta(r) \phi_c(r) \tag{5.3}$$

where $\phi_c(r)$ is the core level wavefunction $\Delta(r) = (\frac{-i}{c})\mathbf{A}(\mathbf{r})$ is the electron photon interaction, Y_L is a spherical harmonic (L=l, m) and $R_l(r,E)$ is the regular solution of the radial Schrödinger equation at energy E for the isolated muffin-tin potential of the excited atom which matches smoothly to the external solution.

It is important to note that the muffin tin potential is not evaluated self-consistently, and there is no mechanism for charge-transfer between atoms. The muffin-tin potential approximation works best for close packed structures, but has been found to be a good

enough approximation for other materials [3]. Work by Weng and Rez [14] was able to show that charge transfer had little effect on calculated near-edge structure, which was more sensitive to coordination. In this work the muffin-tin radii from each atom was determined by matching the potential at the boundary with that of the neighbouring atom, although others have used half the nearest neighbour distances [15] with good results.

5.3.2.1 Z+1 Approximation

In some cases, the best fit to experiment was obtained by using the next atom up in the periodic table as the absorbing atom. This procedure is known as the Z+1 approximation and attempts to take into account the effect of the core-hole [16]. The core-hole is the effective "increase" in nuclear charge of the ionised or absorbing atom. As discussed above the muffin tin potential was not calculated self-consistently and this reduces the accuracy of low lying unoccupied states, which are dominated by valence electron effects. The "Z+1" approximation has been used successfully to treat several systems, while some authors have found a superior fit to experimental data using a neutral central atom as [4]. A variant on the (Z+1) approximation is the (Z+1)* approximation, where the (Z+1) absorbing atom is treating as having a 1s electron promoted to a higher orbital. For example if the (Z+1) approximation is applied to a carbon atom, (Z+1) is nitrogen. A simple (Z+1) has the electronic arrangement of $1s^2 2s^2 2p^3$ whereas the (Z+1)* is $1s^1 2s^2 2p^4$. This was tested for each structure and it was found either the normal (Z+1) or neutral central atom gave the best fit to experiment.

5.3.3 Evaluation of Multiple Scattering

The multiple scattering calculation considers all paths between the central and surrounding atoms as described by Vvedensky *et al.* [9]. Rather than try and invert the entire scattering matrix, the real-space cluster is divided into a series of concentric rings and the scattering of each successive ring is calculated recursively. The MS includes a calculation of both intershell and intra-shell scattering. Within the calculation the incident "photon" is considered to be circularly polarised, which means that any

comparison must be made to a polycrystalline sample.

The final step of the MS calculation is to sum each of the angular momentum components ($j = 0, \pm 1$) and add to transition matrix element. All calculations used a inelastic attenuation parameter (V_i=-0.5eV) to represent experimental broadening. Details of all the calculations are shown in Table 5.1.

5.4 Results and Discussion

In the following sections, the ELNES calculated using multiple scattering is shown below each experimental edge, aligned in energy to the first EXELFS peak. Some alignment is necessary since the Fermi energy in multiple scattering calculations is not accurately determined. The Fermi energy is not accurately determined because the energies of the unoccupied states is not known precisely.

5.4.1 Diamond and Graphite Carbon K- edges

Fig (5.5) shows the carbon K-edges for (i) glassy-carbon and (iv) crystalline diamond. Diamond and glassy-carbon have remarkably different experimental K-edges, as shown in Figure 5.5, reflecting the differences in structure and bonding of the two materials.

For glassy carbon, it can be seen that the agreement between theory and experiment is reasonably good. The multiple scattering calculation with a Z+1 approximation correctly predicts the presence of three main features present in graphite: the sharp 1s – π^* peak at 285eV (A); the broad σ^* peak from 290-310eV (B) and the first EXELFS peak at about 226eV (D). The differences between multiple scattering calculation and the experimental NES are: (i) the relative intensity of the major peaks, (ii) the energy difference of the pre-edge 1s – π^* and (iii) some differences in fine structure A summary of the energy of the major feature in the experimental and calibrated NES are shown in Table 5.2.

The disparity in the relative intensities, especially close to the Fermi energy, is a problem inherent in these calculations due to the non self-consistent nature of this method. Despite this problem, the calculated and experimental edges of graphite are quite sim-

ilar and compare favourably to other calculations of the same type [17, 15].

The calculated diamond NES shows the absence of the 1s – π^* resonance (seen in glassy carbon) as expected since crystalline diamond has only covalent σ bonds. The diamond experimental K-edge shows three distinct peaks labelled A, B and C (D being the first EXELFS peak). Comparing the experimental and calculated K-edges (Table 5.1) it can be seen that the features are correctly located within 1-2eV of the correct value. The relative intensities of peaks A, C and D also compare well.

For diamond and graphite multiple scattering theory successfully predicts the positions of the major EEL spectral features. However the relative intensity of several peaks in the multiple scattering calculations were different from that observed experimentally, and some detailed fine structure was not reproduced correctly. However, the calculations were successful in predicting major differences of diamond and graphite NES including (i) the presence of the 1s – π^* resonance and (ii) the general shape and position of the major spectral features of the 1s – σ^* states.

Material	Number of Atoms	Cluster Size (Å)	Number of Shells	Absorber	Radius of Muffin Tin
Diamond	98	5	9	neutral	r_C=0.77223 Å
Graphite	140	7.1	20	(Z+1)	r_C=0.70889Å
c-BN	122	5.3	11	neutral	r_B=0.78266Å
					r_N=0.78266Å
h-BN	129	6.7	17	(Z+1)	r_B=0.71810Å
					r_N=0.72757Å
$\beta - C_3N_4$	69	4.7	17	neutral	r_C=0.73831Å
					r_N=0.70831Å
$\beta - Si_3N_4$	71	5	9	neutral	r_{Si}=0.92395Å
					r_N=0.78731Å

Table 5.1: The materials for which ELNES was calculated using the MS technique - the muffin-tin radii r_i were chosen to provide the smoothest overlap between adjacent atoms.

		Experimental Position (eV)					Multiple scattering (eV)				
Material	K-Edge	A	B	C	D	E	A	B	C	D	E
Diamond	C	291	297	304	325	-	293	-	303	327	-
Graphite	C	285	292	-	327	-	286	290	-	327	-
c-BN	B	193	210	226	-	-	194	207	-	226	-
	N	409	423	439	-	-	411	424	-	439	-
h-BN	B	186	194	199	210	-	187	195	200	210	-
	N	400	407	415	425	439	400	409	415	428	441
$\beta - Si_3N_4$	N	406	429	-	-	-	410	429	-	-	-

Table 5.2: The MS calculated peak positions compared to the same experimentally determined features in the ELNES for the materials in Table (5.1)

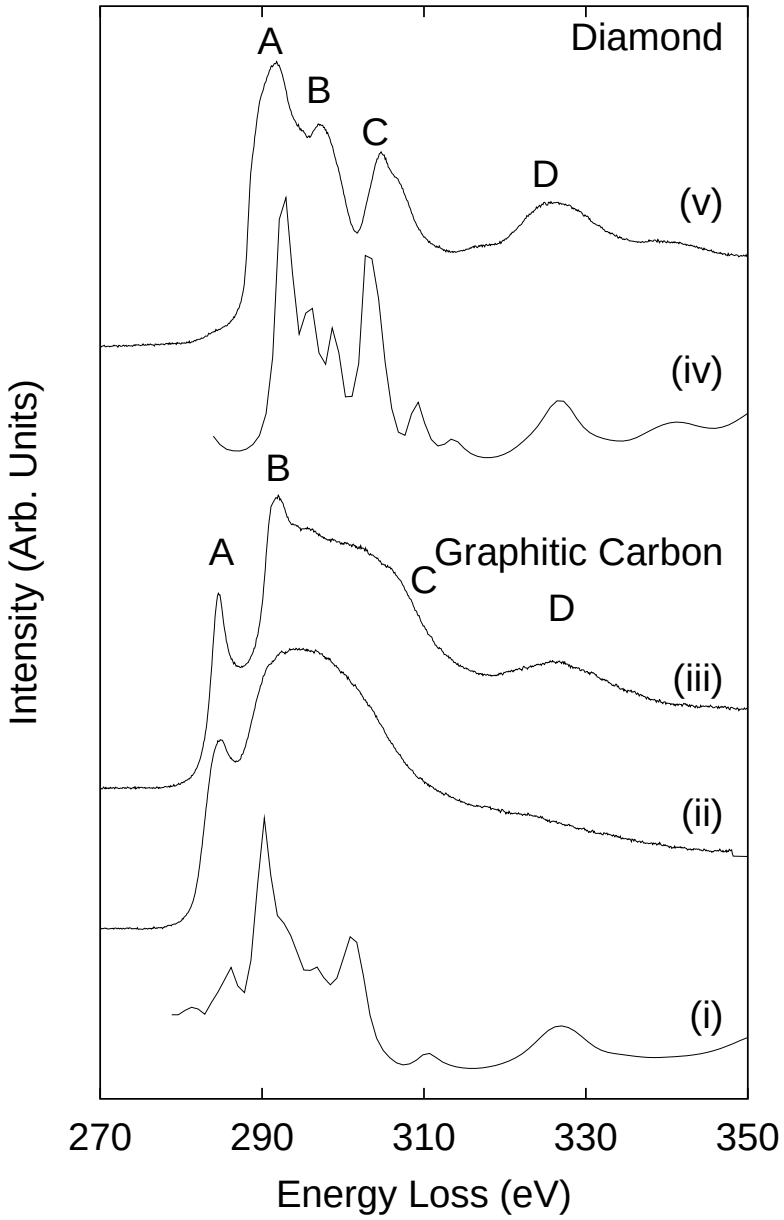

Figure 5.5: The carbon K-edge calculated using MS for (i) graphite and (iv) diamond compared to those experimentally measured for (ii) $a-$C, (iii) glassy carbon and (v) crystalline diamond.

5.4.2 Boron and Nitrogen K-edges in h-BN and c-BN

Structurally analogous to diamond and graphite, two of the crystalline structures for boron nitride, c-BN and h-BN (known as white graphite) are the next structures studied. As shown in fig (5.6), the experimental B K ELNES for both (iv) c-BN and (ii) h-BN are very different to the carbon K-edges shown in fig (5.5).

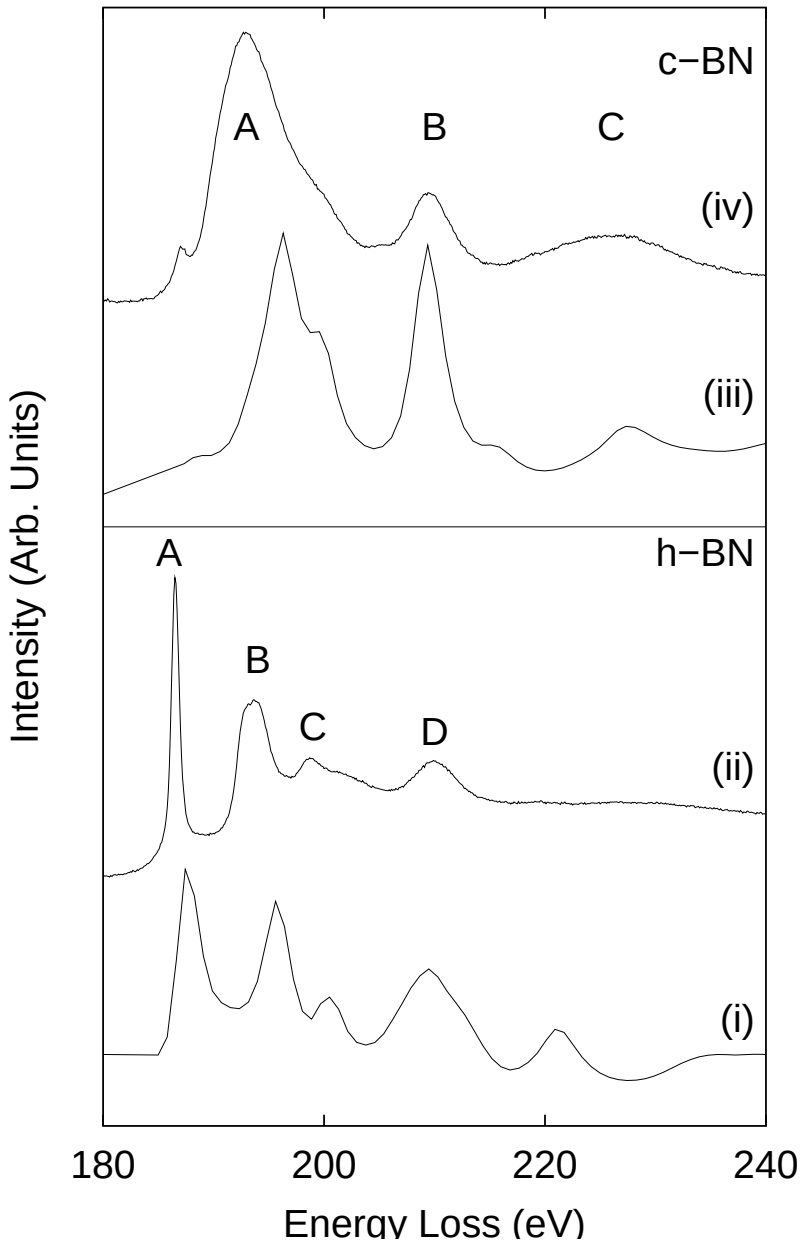

Figure 5.6: The MS calculated and experimental B K ELNES for hexagonal and cubic Boron Nitride.

As was the case with graphite, the best fit with experiment was obtained using a Z+1 approximation for h-BN. The position of the peaks A (π^*), B and C are within 1-2eV of the experimental values. The 1s – π^* feature is noticeably more intense in h-BN than in graphite due to less electron screening producing a more stable (therefore more easily excited) 1s – π^* closer to the Fermi level. All experimental peaks in h-BN are reproduced by the calculation, the disparity between the energy of peak B could be due to the calculation not picking up the splitting of this peak.

The experimental Boron K-edge of c-BN shown in Figure 5.6 shows three distinct peaks. The small pre-edge π^* feature is not normally present on a c-BN B K-edge and may be due to some h-BN contamination in the experimental sample. The multiple scattering calculation successfully predicts the overall shape of the edge. The corresponding Nitrogen K-edges for h-BN and c-BN are shown in Figure 5.7. The results for the nitrogen K-edges are similar to the boron K-edges with major spectral features reproduced in the multiple scattering calculations.

5.4.3 Nitrogen K-edges in Carbon and Silicon nitride

As there is no available ELNES measurements for $\beta - C_3N_4$, it is not possible to compare our calculation with experiment. However, we can use $\beta - Si_3N_4$ (from which the structure $\beta - C_3N_4$ was predicted), to obtain a comparison between calculation and experiment, and infer the key features of the $\beta - C_3N_4$ ELNES. In the following section, experimental nitrogen K-edges for $\beta - Si_3N_4$ are compared to those calculated by multiple scattering. Also the experimental K-edge from nitrogen in amorphous carbon nitride deposited using cathodic arc (See Section 3.2.4) is compared to multiple scattering calculations for $\beta - C_3N_4$.

Considering the ELNES of nitrogen in $\beta - Si_3N_4$ shown in fig (5.8) we see that the multiple scattering calculation has predicted the main features of the edge, although the calculation does predict some fine structure which is not apparent in the experimental spectrum. However, the calculation has successfully placed both A and B (to within a few eV) and reproduced the asymmetry of the first peak (A).

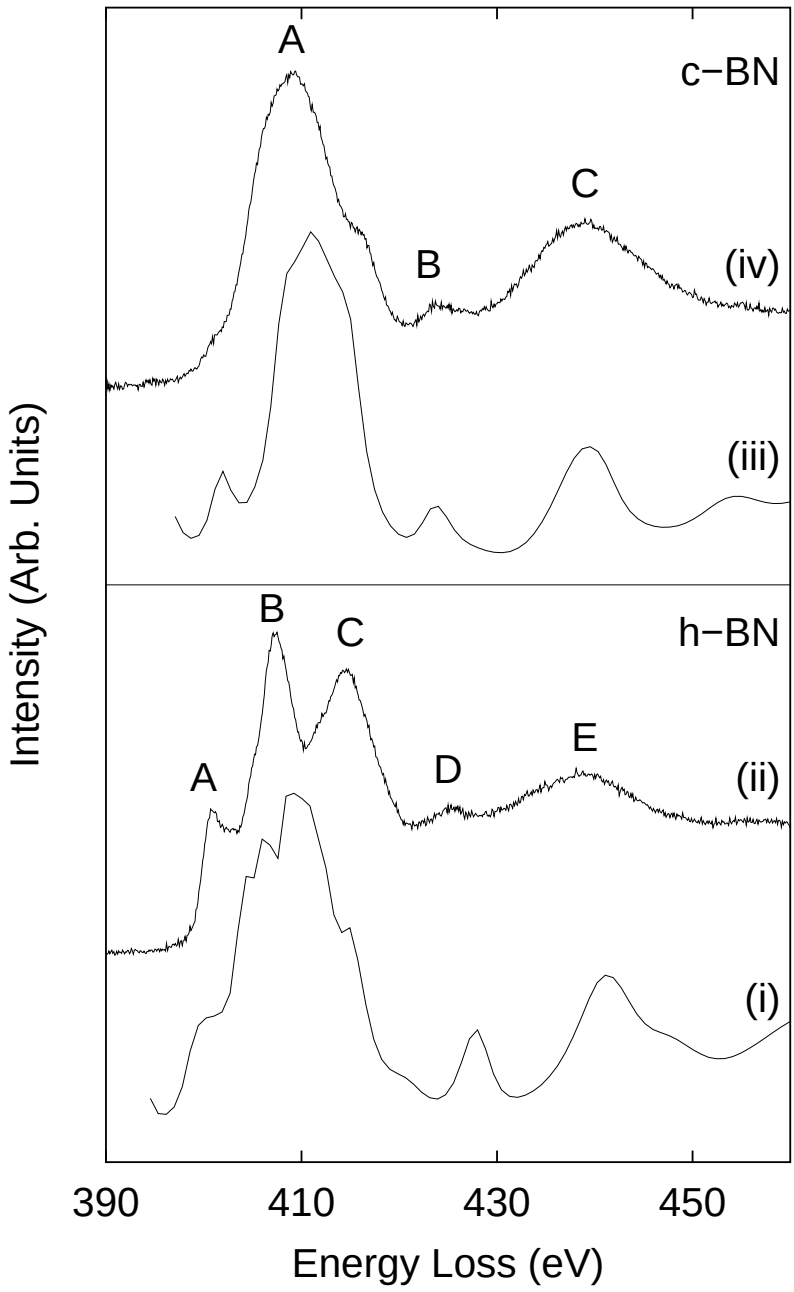

Figure 5.7: The MS calculated ELNES and experimental nitrogen K-edges for hexagonal and cubic Boron Nitride.

Moving to the experimental amorphous CN_x nitrogen edge in fig (5.8)(iv), we see a very different edge compared to silicon nitride. First, there is a 1s – π^* (A) feature indicative of local sp^2 bonding, and the 1s – σ^* peak (B) is much broader than the N K-edge in silicon nitride. The features present and their relative intensities strongly

suggest that the nitrogen is bonded in a graphitic-like environment. This result led to the suggestion that the amorphous CN_x material consisted of nitrogen bonded largely into sp^2 sites as discussed in Section 3.5.

In order to explore the possibility that the N K ELNES could also be consistent with that expected from the $\beta - C_3N_4$ structure, we compare the experimental edge with that calculated using multiple scattering theory in Figure 5.8. There is little similarity between the calculated nitrogen K-edge of $\beta - C_3N_4$ and that observed in the cathodic arc deposited CN_x consistent with our interpretation that the structure of this material is graphitic in nature (See Section 3.5). However, due to the relatively good agreement between experiment and calculation in the other materials studied, we expect that the NES of nitrogen in $\beta - C_3N_4$ structure will resemble that shown in Figure 5.8. Therefore this calculated edge provides a means of identifying the presence of $\beta - C_3N_4$ synthesised experimentally.

5.5 Comparison of β-C_3N_4 C and N K edge ELNES to c-BN and diamond

In fig (5.9) the C K edge ELNES for MS calculated β-C_3N_4 is shown compared to a calculation for diamond. The character of the ELNES for the C K edge is essentially the same as the diamond, although the principal σ^* peak is broadened and the secondary σ^* peaks are attenuated compared to diamond. This may be due to the reduced symmetry of the carbon location in β-C_3N_4, surrounded as it is by two different N sites, neither of which are four-fold coordinated.

The comparison of the N K edge ELNES in fig 5.10 of β-C_3N_4 and c-BN, shows that the bonding in these two materials is likely to be similar and the N K edge of β-C_3N_4, should it be synthesised, will bear a strong resemblance to the c-BN N K edge ELNES. The degree of ionicity in c-BN has not significantly affected the ELNES, and the lower degree of ionicity in β-C_3N_4 should equally not significantly alter the edge shape.

The C K ELNES for β-C_3N_4 and diamond can be further compared by looking at the evolution of features in the spectra on a shell by shell basis. This is shown in figs(5.11)

and (5.12). Wibbelt *et al.* suggested that a possible explanation for the attenuation of features beyond the major σ^* peak was in non-tetrahedral (or incomplete) coordination of the nitrogen atoms. Comparing figs(5.12) and (5.11) we can see that the second shell of atoms in diamond produces the pronounced second peak. The β-C_3N_4 exhibits no splitting at this shell. In diamond the second shell consists of twelve atoms at 2.52 Å, whereas in β-C_3N_4 the second shell is only two N at 2.40 Å. The third shell in β-C_3N_4 however is six C atoms at 2.52 Å. In diamond, the multiple scattering between C atoms of the second shell (see fig (5.12)) increases the intensity of the second σ^* peak. In β-C_3N_4, the multiple scattering between the atoms of the third shell (not shown) has little effect on the spectra. Rather than simply a difference in coordination, the hexagonal structure, distance, and relation of atoms within the shell has reduced the β-C_3N_4 C K ELNES intensity beyond the first σ^* peak.

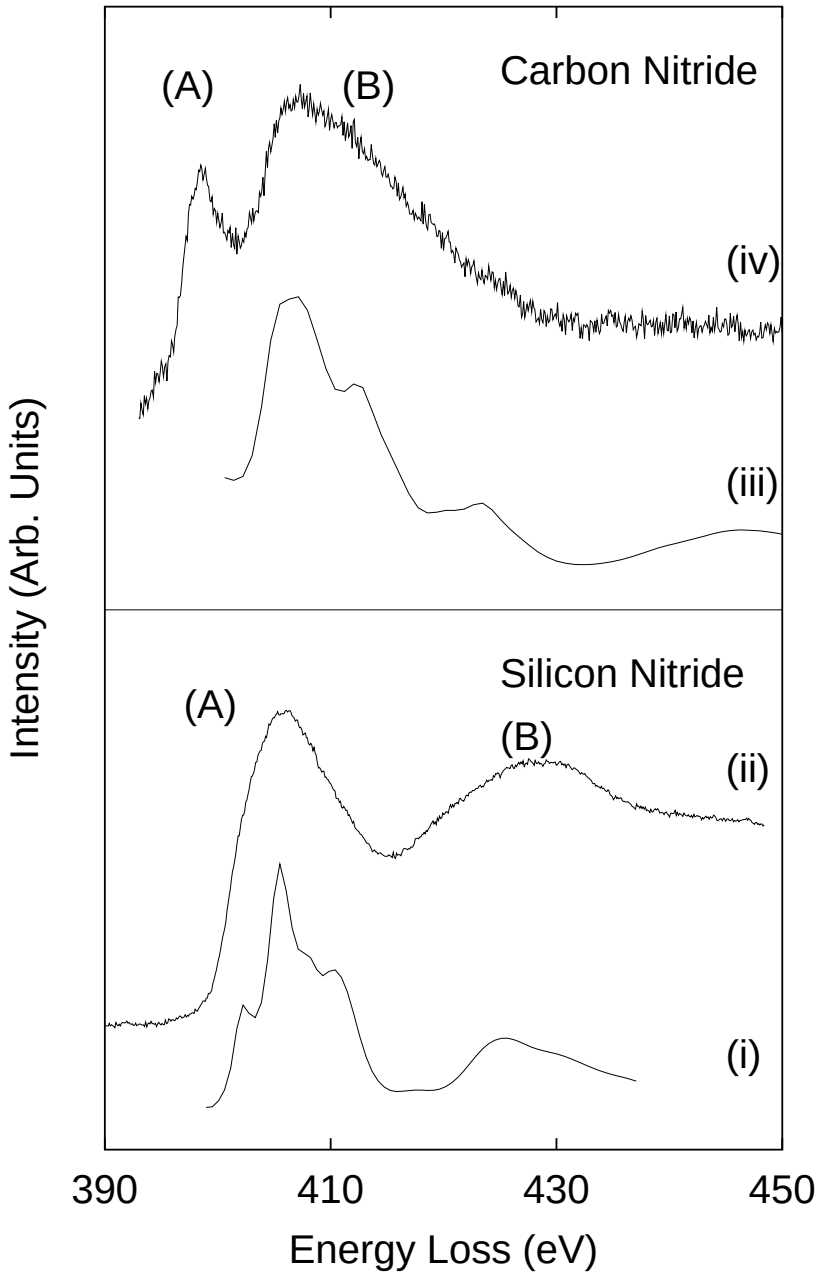

Figure 5.8: (i) The calculated nitrogen K-edge in $\beta - Si_3N_4$ and (ii) the experimental edge of the same, with (iii) the calculated nitrogen K-edge in $\beta - C_3N_4$ and (iv) the nitrogen K-edge of amorphous carbon nitride deposited using a cathodic arc.

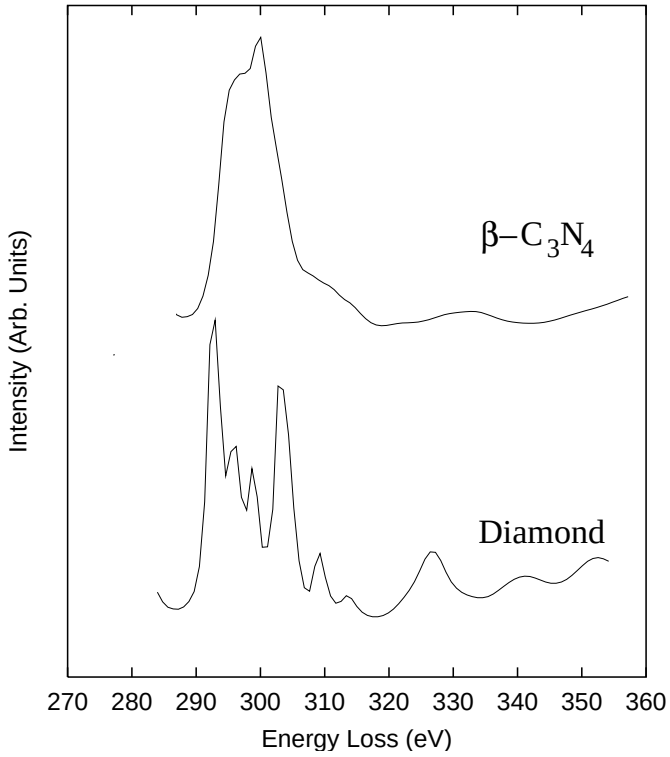

Figure 5.9: A comparison of the C K ELNES for diamond and theoretical β-C_3N_4 (Liu *et al.* 1994).

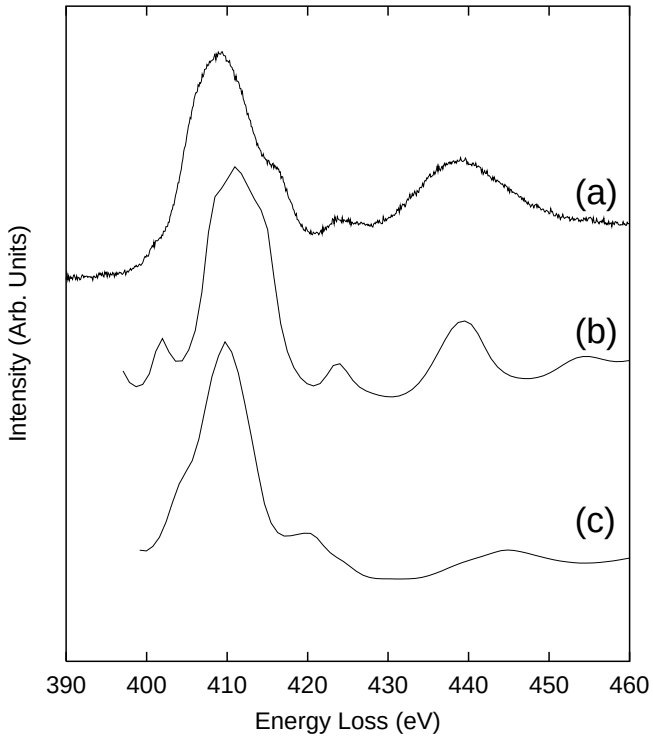

Figure 5.10: A comparison of the N K ELNES for c-BN and theoretical β-C_3N_4 [18]. The two separate plots for β-C_3N_4 are because there are two unique N sites in the β structure, these were summed to give the spectra shown in fig(5.8)

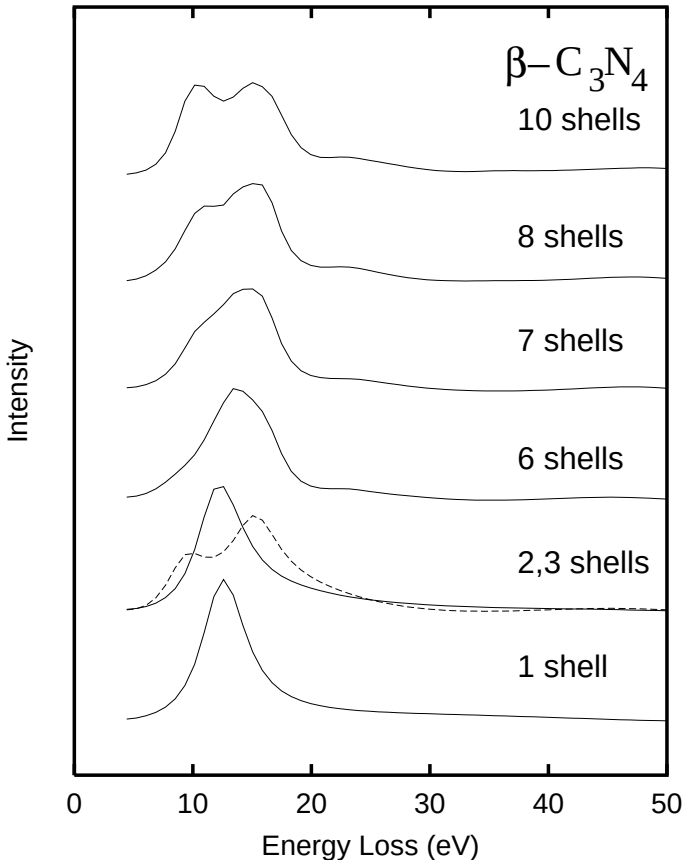

Figure 5.11: A shell-by-shell look at the C K ELNES for theoretical β-C_3N_4 (Liu and Wentzcovitch, 1994)

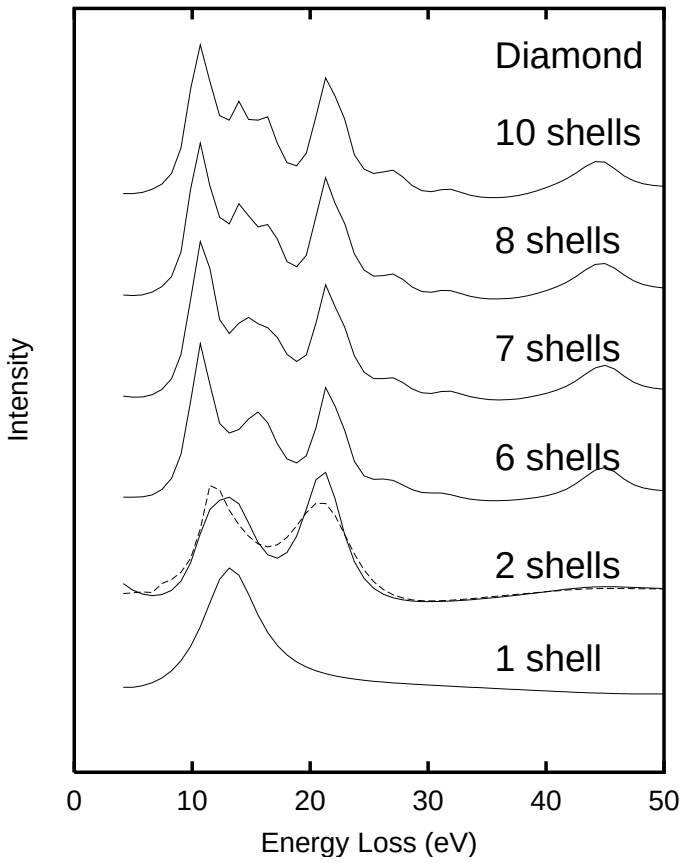

Figure 5.12: A shell-by-shell look at the C K ELNES for diamond. The plot labelled 2,2' shells indicates full multiple scattering (solid) line and single scattering between central atom and shell only (dotted).

5.6 Conclusions

We have found that NES calculated using multiple scattering theory provides good agreement with experiment for diamond and graphite, cubic and hexagonal boron nitride and silicon nitride. Multiple scattering theory successfully predicted the positions of the major spectral features, although fine details are not always reproduced well.

The discrepancies between experiment and calculation are probably due to the non-self consistent nature of the potential employed. The multiple scattering calculation for the nitrogen K-edge in $\beta - C_3N_4$ was not similar to that of cathodic arc deposited CN_x, confirming the conclusion that the structure of this material is not consistent at all with that expected from $\beta - C_3N_4$.

The predicted ELNES for C and N K edges in β-C_3N_4 should resemble the C K ELNES in diamond and N K ELNES in c-BN. These spectra may prove useful in attempts to identify unknown phases of crystalline carbon nitride.

This work shows that calculations based on multiple scattering theory are of sufficient accuracy to provide information on the edge structure associated with the materials studied.

Bibliography

[1] R. F. Egerton, *Electron Energy Loss Spectroscopy in the Electron Microscope*, 2 ed. (Plenum Press New York, 1996).

[2] R. A. Rosenberg, P. J. Love, and V. Rehn:91, Phys. Rev. B **33,** 4034 (1986).

[3] R. Brydson, EMSA Bulletin **21,** 57–67 (1991).

[4] *Transmission Electron Energy Loss Spectroscopy Materials Science*, M. M. Disko, C. C. Ahn, and B. Fultz, eds., (The Minerals, Metals and Materials Society, 1992).

[5] H. K. Schmid, Microscopy, Microanalysis and Microstructure **6,** 99–111 (1995).

[6] P. Redlich, F. Banhart, Y. Lyutovich, and P. M. Ajayan, Carbon **36,** 561–563 (1998).

[7] J. L. Beeby, Proceedings of the Royal Society London, Series A **A302,** 113 (1967).

[8] P. J. Durham, J. B. Pendry, and C. H. Hodges, "Calculation of X-ray absorption near edge structure, XANES," Computer Physics Communications **25,** 193 (1982).

[9] D. D. Vvedensky, D. K. Saldin, and J. B. Pendry, "An update of DLXANES, the calculation of X-ray absoprtion near-edge structure," Computer Physics Communication **40,** 421 (1986).

[10] R. Brydson, "Private Communication,".

[11] F. Herman and S. Skillman, *Atomic Structure Calculations* (Prentice Hall, New York, 1963).

[12] L. F. Mattheiss, Physical Review **134,** A970 (1964).

[13] K. Schwartz, Physical Review B **5,** 2466 (1972).

[14] X. Weng and P. Rez, Physical Review B **39,** 7405 (1989).

[15] M. Wibbelt, H. Kohl, and P. Kohler-Redlich, Physical Review B **59,** 11739–11745 (1999).

[16] X. Weng, P. Rez, and H. Ma, Physical Review B **40,** 4175 (1989).

[17] D. G. McCulloch and R. Brydson, Journal of Physics-Condensed Matter **8,** 3835 (1996).

[18] A. Y. Liu and R. M. Wentzcovitch, Physical Review B **50,** 10362–10365 (1994).